Geological Structure and Possible Mineralized Zones in Ikungi – Manyoni Area, Tanzania: Delineated from High-resolution Aeromagnetic Data

Raymond K Pius[*1,2] and Michael M Msabi[1]
[1]Department of Geology, University of Dodoma, P. O. Box 259 Dodoma, Tanzania.
[2]Geological Survey of Tanzania, P. O. Box 903, Dodoma, Tanzania.
*Corresponding author: raypiusmatiku@yahoo.com; Co-author: mmsabi@yahoo.com

Abstract

Understanding geological structures is important in mineral exploration. Delineating subsurface geological structures, structural intersections, and complexities of potential geological settings for the formation of hydrothermal mineral deposits, such as gold requires using magnetic data, particularly, high-resolution aeromagnetic data. To define possible targets for mineral exploration, this study used linear detection and the Centre for Exploration Targeting (CET) techniques on high-resolution aeromagnetic data for structural delineation and interpretation. The study's conclusions indicate that the majority of geological features, such as faults, shears, fault intersections, and fracture systems, trend NE-SW, N-S, and occasionally NW-SE. These structures create potentially large areas that have a strong chance of becoming mineralized. The CET grid analysis technique defined mineralized zones, particularly the structural intersections which are potential targets in mineral exploration. The effectiveness of the CET technique in mineral prospecting was demonstrated by the correlation between the results and existing mineral occurrences (such as Shanta Gold Mine, abandoned pits, and the operating pits of small-scale miners in Muhintiri). Based on the findings reported herein, any sites that share characteristics with those that have demonstrated gold mineralization should be prioritized for ground follow-up.

Keywords: High-resolution aeromagnetic data; CET technique; Structural delineation; Mineralized zones and Ikungi – Tanzania.

Introduction

High-resolution aeromagnetic data are critical in mapping basement geology through cover and, most importantly, in a self-sufficient and accurate manner, it is a valuable tool for greenfield exploration of various commodities. The ground selection stage of unexplored and/or underexplored areas is critical in any greenfield mineral exploration program (Hronsky and Groves 2008). A crucial first step in promoting greenfield exploration in nations like Tanzania is acquiring high-resolution aeromagnetic data over large areas. Second step, these datasets should be interpreted and made available at a minimal or no cost to mineral explorers, especially small and medium-scale operators. By interpreting these data, one can identify which areas have the potential for mineral occurrences/deposits and seek for license.

Several hydrothermal mineral deposits have a strong spatial association with faults, shear zones and other crustal discontinuities in a wide range of scales (Groves et al. 1998, Sillitoe 2000, Goldfarb et al. 2001, Bierlein et al. 2006, Austin and Blenkinsop 2009). Yet, it is the small-scale faults that are close to the large-scale geological structures that are more

plausible for mineral deposit formation (Bierlein et al. 2006), which act as pathways for controlling fluids to the upper crust and/or within the crust (Sibson et al. 1988, Cox et al. 2001, Chernicoff et al. 2002). In the localised mineral occurrence areas, there is a strong correlation between small-scale geological structures and those mineral deposits. These structures act as conduits of the hydrothermal fluids carrying metals and metalloids in solution, including elements such as gold, copper, silver, lead, zinc, arsenic and dissolved gases, among others, which precipitate to form valuable ore deposits. Therefore, it is imperative to explore new mineral deposits in areas close to the small-scale structures. These faults are commonly associated with major lineaments defined by potential field gradients (where rocks of contrasting density and/or magnetic susceptibilities are differentiated) (Bierlein et al. 2006). Spatial relationships between magnetic and gravity conduits (major geophysical lineaments) and mineralization have been recognized (Bierlein et al. 2006).

To delineate and understand geological structures, especially small-scale lineaments and lithological boundaries, geophysical surveys have played a big role in studying the physical properties of the surface and subsurface geology by employing low- and high-resolution airborne data sets (Dentith and Mudge 2014, Alarifi et al. 2019, Kumwenda and Lackie 2019). Despite the presence of small and medium-scale miners and low-resolution aeromagnetic data acquired in the study area, there is no detailed delineation of small-scale structures. Further, the interpretation of low-resolution data has suffered several limitations in delineating small-scale structures, which are significant in hosting localised mineralization. For that reason, low-resolution data have been less preferred in detailed local-scale exploration works, hence, explorers resorted to high-resolution data for delineating small and concealed geological features (Mgundulwa 2007). Noteworthy, high-resolution geophysical data can also be integrated with geological mapping, assays from rock, stream sediment and soil samples, to define and increase confidence in mapping lithological units, structures, and target zones associated with mineralization (Tounkara et al. 2017, Kumwenda and Lackie 2019).

This study therefore uses high-resolution aeromagnetic data to delineate the subsurface geological structures and hence, define gold mineralized zones in the study area. These findings further, provide insight to small-and medium-scale miners who normally have limited resources to conduct detailed exploration programs.

Geological Setting
Regional geological setting
The study area is located in central Tanzania and is characterized by the presence of the Archaean Tanzanian Craton. The craton is bordered by five lithostratigraphic and tectonic units, such as the Palaeoproterozoic mobile belts of Ubendian and Usagara on the west-southwest, south and southeast margin, the Mesoproterozoic Karagwe-Ankolean belt to the west, the Neoproterozoic Mozambique belt to the east and finally, the Neoproterozoic Malagarasi Super-group to the west of the craton, respectively (Cutten et al. 2006, Thomas et al. 2013, Thomas et al. 2014). Kabete et al. (2012a) and Kabete et al. (2012b) carried out an extensive review of the Archaean Tanzanian Craton in terms of the tectonostratigraphic and metallogenic outlooks. As a result, based on the difference in lithotectonic and age, the Archaean Tanzanian Craton was sub-divided into several WNW-ESE trending superterranes which were strongly reworked during the Neoproterozoic East African orogeny particularly at the margins in the south and east of the East African Orogen (Cutten et al. 2006). These superterranes are grouped into two sub-groups, namely; the Lake Victoria region and the central Tanzania. Central Tanzania is composed of four superterranes: (a) the Moyowosi-Manyoni Superterrane; (b) Dodoma Basement Superterrane; (c) the Dodoma Schist Superterrane, and (d) the East Ubendian-Mtera Superterrane (Kabete et al. 2012b). The central Tanzania region is largely made up of the amphibolites-facies terranes which host hypozonal gold systems (Groves et

al. 2003, Kisters et al. 1998) in the relative interlaminations of quartz veins in wide ductile shear zones. This region has relatively three small-scale but significant gold systems, such as (i) Mwenge in the Moyowosi-Manyoni Goldfields, (ii) Madengi Hills and Mafulungu (Barth et al. 1996) in the Dodoma Basement Goldfields (Kabete 2008), and (ii) Kitunda in the Dodoma Schist Goldfields, comprising hypozonal gold systems hosted by the mafic-amphibolite and/or granitoid gneisses (Kabete et al. 2012b).

Local geology
The study area is located within the Quarter Degree Sheet (QDS) Number 122 (Figure 1), the geological framework of the area corresponds to that of the Archaean Tanzanian Craton, particularly the central Tanzania region. It is a heterogeneous crystalline basement terrane composed of belts of low metamorphic grade metavolcanic and metasedimentary rocks collectively known as greenstones. This basement is surrounded by higher grade amphibole granitic gneiss incorporating variably deformed older granite intrusions, and cross-cut by younger Neoarchean granitoid (Kashabano et al. 2003). The ancient rocks in the study area are mainly of granitoids. They are of different types distinguished by composition, structure and texture. According to their age, there are two groups of granitoids, old and young. The old granite >3.1 billion years (Ga) consists of five members puma granitic gneiss, muhintiri granite, ikungi granitic gneiss, piani granitic gneiss and Isuna granite. The young group of approximately 2.5 Ga age is represented by Ipuli and Manjaro granites. The Neogene Lake sediments (Kilimatinde "cement") cover the larger part of the study area under consideration.
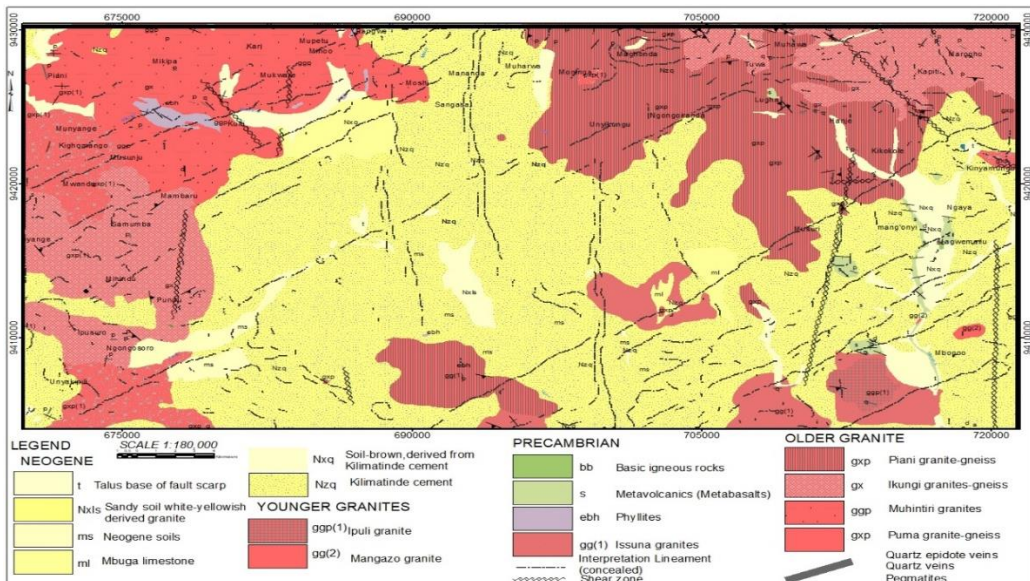

Figure 1:   The updated geological map of the study area with structures and lithological units (Modified after Kashabano et al. 2003 and Msechu 2019).

Methods and Materials
High-resolution aeromagnetic data: Acquisition
The high-resolution aeromagnetic data used in this study were acquired in 2012 under the supervision of the Geological Survey of Tanzania (GST) by Sanders Geophysics Limited of Canada. The aircraft-mounted with magnetic, gravity and radiometric sensors flew at the flight height of 60 m above the ground with a spatial resolution of 50 m x 50 m which is one-fifth of the survey line spacing of 250 m. The airborne sensors were mounted in a fibreglass stinger installed in the tail of the

aircraft. The traversing and tie lines were aligned in north-south and east-west directions, respectively. The airborne instrument system used was a non-oriented (strap-down) optically-pumped caesium split-beam sensor with a sensitivity of 0.005 nT, a range of 20,000-100,000 nT and a sensor noise of less than 0.02 nT. Total magnetic field measurements were recorded at 160 Hz in the aircraft and then later decimated to 10 Hz in the processing.

High-resolution aeromagnetic data: Processing

The data processing followed a standard workflow in three stages to produce the magnetic anomalies corresponding to the subsurface geological causative bodies (Luyendyk 1997). The three stages of processing aeromagnetic data are such as (i) Stage I: importing datasets into the software, (ii) Stage II: removing systematic line-levelling errors, (iii) Stage III: statistical and full levelling with the major objective of adjusting the survey lines so that all lines match the trend tie-lines exactly at each intersection. Data importation and cleaning were done in the Oasis Montaj software package version 8.4, followed by residual field calculation by subtracting IGRF from the total magnetic data. The input IGRF model of 2010 was used because the IGRF standards are given after every 5 years. Finally, the obtained database and grid diagrams that reflect the magnetic anomaly of geological causative bodies are enhanced by various filtering techniques (Figure 2).
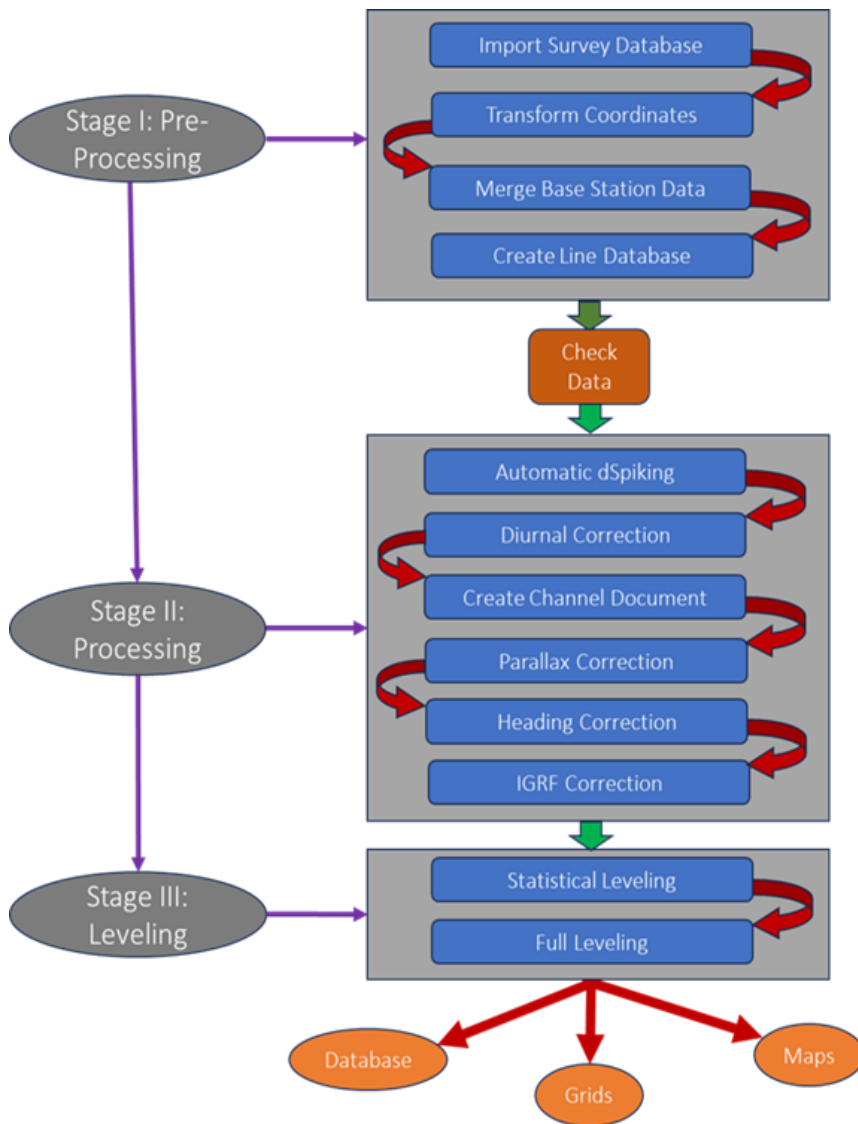
Figure 2: Schematic workflow of the magnetic data processing procedures.

Total magnetic intensity (TMI) data were gridded using the minimum curvature technique described by Briggs (1974) and Swain (1976). A grid cell size of 65 x 65 m, one-fourth (1/4) of the flight line spacing, is to avoid short-wavelength errors that may misinterpreted as lines perpendicular to the line direction (Dentith 2011, Anudu et al. 2014). Dentith (2011) proposed that grid cell size (i.e. distance between interpolated points) should be in a range of 1/3 to 1/5 of the survey line spacing. This is to enhance geological boundaries or internal structural patterns of geological units and accentuate lineaments associated with faults, contacts, fractures, or shear zones.

The TMI grid data were then transformed using a reduction-to-pole (RTP) filter (Baranov 1957, Blakely 1995), to remove the anomalies due to latitude shift from the centre of the magnetic causative body and hence, correlate magnetic anomalies with geological features. Parameters used in the RTP filter were geomagnetic inclination of -47.3° and

geomagnetic declination of -2.1°. The RTP grid data were further processed to transform and enhance magnetic anomalies associated with the near-surface geological bodies, and structures and enhancing small features.

Vertical derivatives (VD) emphasize short-wavelength (high wavenumber) anomalies and suppress long-wavelength (low wavenumber) anomalies (Dobrin and Savit 1988, Telford et al. 1998). Short-wavelength anomalies are always caused by surface and near-surface causative geological bodies, while long-wavelength anomalies are due to deeper ones. The VD tends to narrow the width of anomalies and detect precisely the lithological contacts/boundaries (Cooper and Cowan 2004). Assuming that the magnetic data were originally RTP, the zero contour values on VD maps should lie exactly across the borders of magnetic source bodies (Reynolds 2011).

The centre for exploration targeting (CET) grid analysis is an extension of the Oasis Montaj software plugin with capabilities to perform texture analysis, phase analysis, and structure detection (Heal et al. 2014, Smith et al. 2019, Uwiduhaye et al. 2021). These are multipurpose algorithms powerful and useful for grid texture analysis, lineament and structural complexities detection, edge detection, threshold detection as well as the definition of exploration target areas. The CET is applied to the RTP grid so that anomalies are shifted over their causative structures and the magnetic susceptibility discontinuities by employing a combination of texture analysis and bilateral symmetric feature detection. Holden et al. (2012) suggested that this structural complexity analysis is useful in locating promising ore deposits. This method highlights regions of discontinuity and analyses structural association to locate intersections, junctions, and changes in strike direction. The extraction of lineaments from the magnetic signal is achieved through three steps, namely, texture analysis, texture ridge detection and thinning of texture ridges (Lam et al. 1992, Holden et al. 2012).

Results and Discussions
Interpretation of large-scale structures and contact boundaries

The total magnetic intensity (TMI) ranges between -71 nT and 101 nT and is characterized by short-wavelength (high wavenumber), medium-wavelength (moderate wavenumber) and long-wavelength (low wavenumber) anomalies. The three anomalous zones are 71 to -20 nT, -20 to 32 nT and 32 to 101 nT termed as Low (L)-blue cloured, Intermediate (I)-green coloured, and High (H)-red coloured, respectively marked on the map (Figure 3). The isolated high anomalies causative bodies are trending in the NE-SW and NW-SE, whereas, the low (blue-cloured) are observed in the northern part. The major structures are also delineated on a geological map of the study area (Semkiwa and Myumbilwa 2013). The locations of structural boundaries are delineated by the TMI signature (Figure 3). The boundaries and exact position of these anomalous signatures are always affected by the presence of remanence magnetization, the same phenomenon has been reported by Ansari and Alamdar (2009).
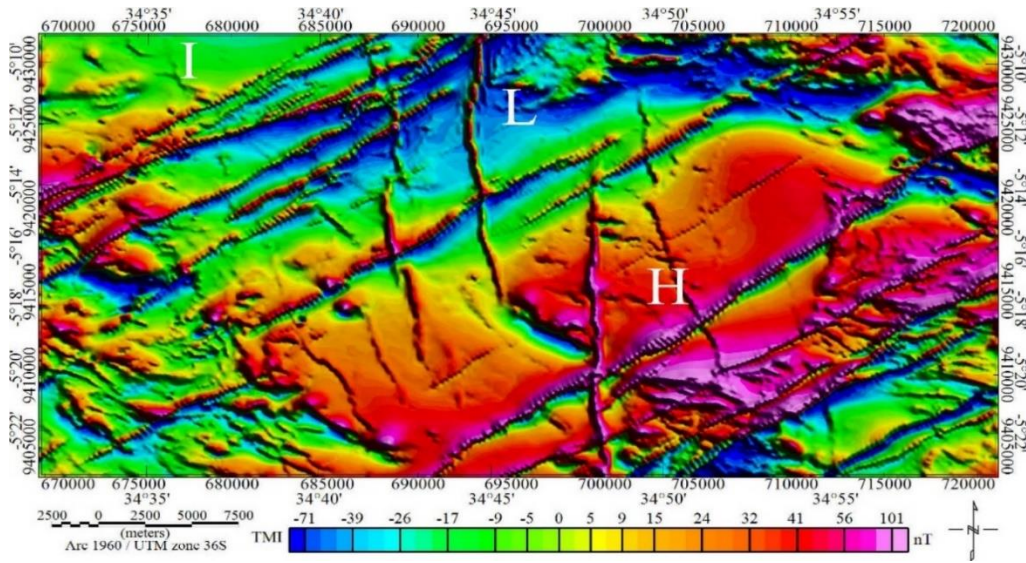
Figure 3: Total magnetic Intensity (TMI) anomaly map showing zones with different magnetic intensities.

The reduction of the effects of the remanence magnetization was carried out by applying a transformation filter (RTP filter) on the TMI signature. The high magnetic intensity areas and linear features trending NE-SW have shown the positive effects of transformation from their original position. Hence, the application of the transformation filter has significantly improved the location and boundaries of the causative bodies (Figure 4). The intensity of the intrusive body on TMI and RTP maps has shown a different shape (Figures 3 and 4). The RTP map shows negative and positive magnetic anomalies.

The central part has intense negative magnetic anomalies with several peaks and linear features of high magnetic intensity trending N-S, NW-SE and NE-SW. These anomalies represent subsurface lineament intrusions of high magnetic content situated at different depths. The improved contacts between magnetic low, high and magnetic susceptible zones possibly are due to deeper sources. The contacts of linear structural bodies are well defined in RTP as compared to TMI (Figures 3 and 4) as also observed by Verduzco et al. (2004).
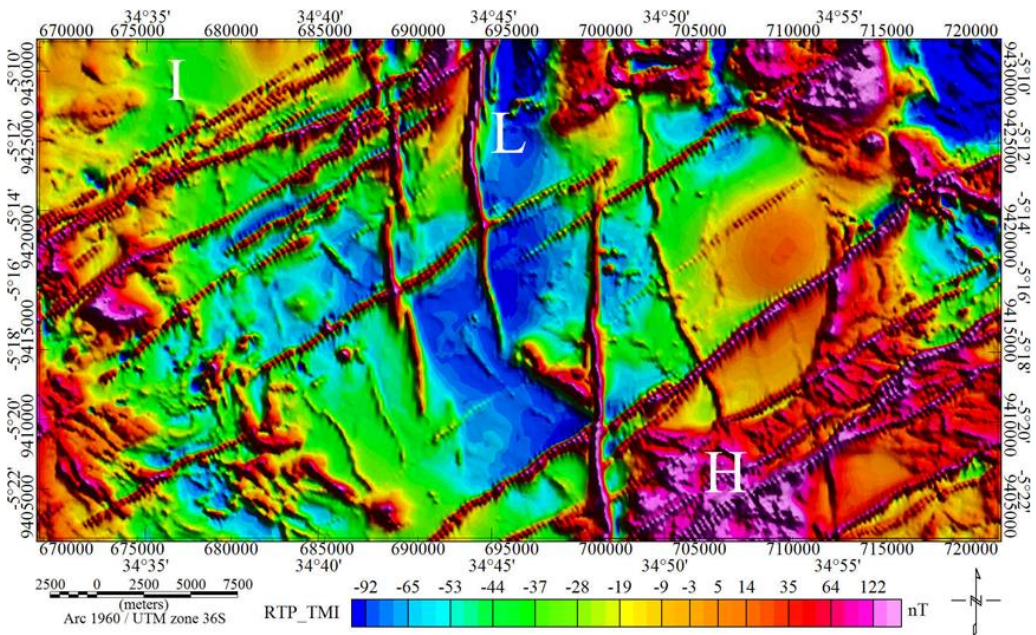
Figure 4: Reduced to the pole map showing the transformation effect caused by the magnetic field of the Earth

However, from the field observation, the high magnetic anomalous zone (H) is related to a younger granite unit containing more magnetic minerals. Moderate to high magnetic anomalous zones are related to older granites such as piani granitic gneiss, ikungi granitic gneiss, muhintiri granite and puma granite gneiss. A relatively low magnetic anomalous zone L is also related to the Neogene soil sediments. The other parts with granitic rocks indicate low magnetic susceptibilities due to the destruction of magnetization as the result of intrusive bodies. Magnetic anomaly signatures, boundaries and structures such as dykes, and faults were defined and delineated, similar findings were reported by Konadu et al. (2018) and Lawal (2020). However, the RTP is inhibited by the presence of remanence because it assumes all magnetization is due to induced magnetization (Milligun and Gunn 1997).

Interpretation of small-scale subsurface structures, complex lineaments and potential mineralized zones

The results from the vertical derivative filter are important in enhancing short-wavelength components of the anomaly while reducing long-wavelength components, which were not delineated on the horizontal gradient map (Konadu et al. 2018). It highlights breaks and discontinuities in anomaly texture and detects the edges and geological boundaries (Jeffrey. et al. 2007). It has shown clear boundaries, more linear structures, discontinuities and displacement trending in NE-SW and N-S directions (Figure 5). In addition, it has delineated small intrusions, geologic structures (dykes and shear zones), similar findings were reported by El-Qassas et al. (2021), and near-surface faults (Ejepu et al. 2018). It is evident that the study area has several faults and is occupied by such short-wavelength anomalies indicating a relatively shallow depth of the causative source.

Linear detection techniques added more detailed information that was not able to be captured by previous filters (Eldosouky et al. 2020). It has delineated trends and discontinuities of linear structures in the study area. With this technique, it was able to establish the structures' characteristics. Characteristics such as brittleness, linear fragmentation and displacement of structures are documented. Structures such as fractures, shear zones and faults were easily identified

due to their brittleness behaviour, linear fragmentation and displacement, respectively.

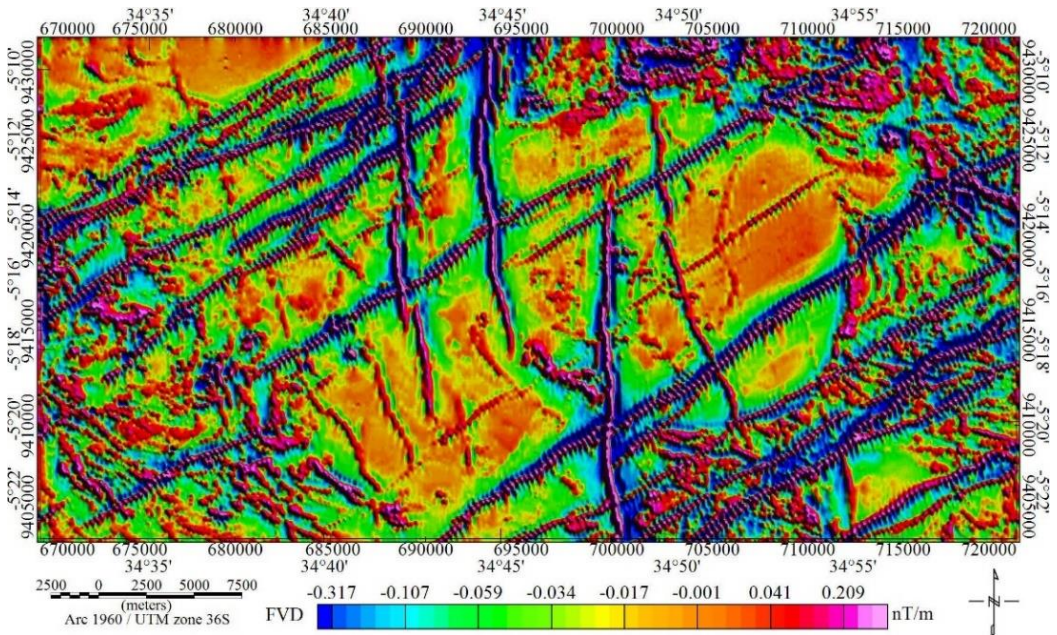A similar observation was made by Fossen and Cavalcante (2017) in their study.

Figure 5: Vertical Derivative highlighting shallow surface magnetic anomalies and intrusive bodies.

The phase symmetry extent calculated from the RTP map is displayed in Figure 6 showing improved linear features and intrusive bodies. As a result, various discontinuity zones are observed and displayed clearly. The symmetry grid produced the local structure map that enables the ridges as well as the valleys to be observed clearly as shown in Figure 6. Holden et al. (2012) reported the same phenomena in their study. Also, the study by Tawey et al. (2019) using a symmetry detection technique identified components of magnetic discontinuity; such as lithological boundaries, faults and dykes.

The linear detection method reveals both enhanced surface and subsurface structural features (faults, shears, fault intersections and fracture systems) (Eldosouky et al., 2020) that mainly trend in the NE-SW, N-S and a few NW-SE directions (Figure 7). The most important and perhaps the youngest trends of these structures extend in the N-S directions because it is characterized by a long length of extension and cutting most of the structures.
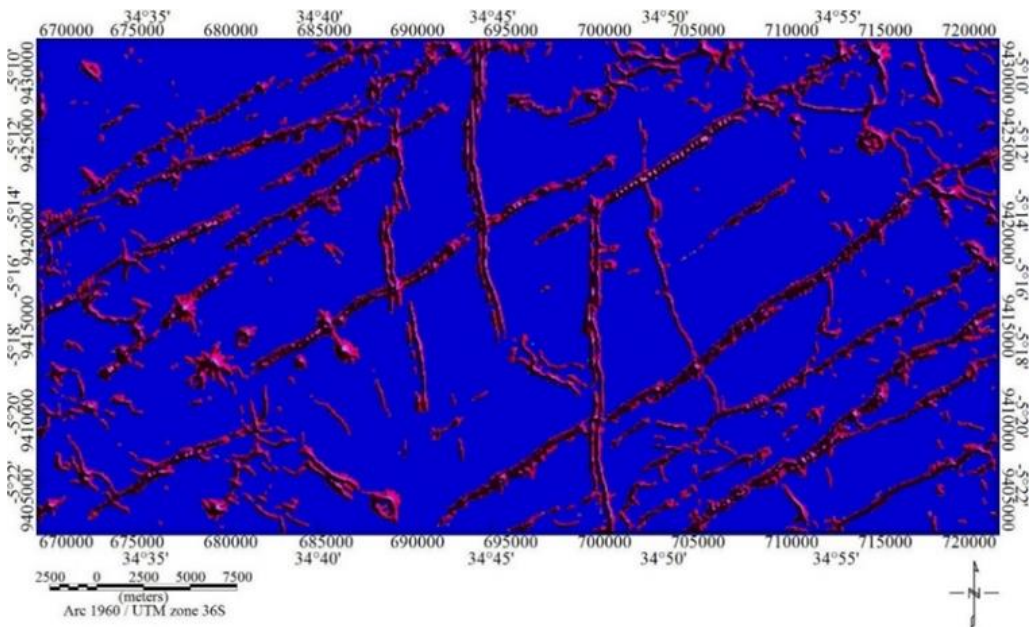
Figure 6:   Phase symmetry derived from the standard deviation image to enhance linear structures.

The oldest phase of the structural lineaments or faults extends in the NE-SW direction that intersects and is displaced by the lateral movement of the youngest structures. Shear zones on the SE and SW parts of the study area are observed from the fragmentation of linear structure resulting from tectonic processes. Faults observed in the study area were produced by downward/descending structure NE-SW slightly displaced by N-S structures and lateral movement in the NW-SE direction. They are associated with the shear zone in the western part of the study area. In their study, Holden et al. (2010) using the same technique reported observation of shear zones and lateral movements of faults. The evidence of faults and the shear zones was also observed during the field visit and documented on the geological map in Figure 1.

To analyse the properties of each structure and produce exploration targets CET was applied. The output was the generation of potential targets with the possibility of being mineralized (Holden et al. 2010). The heat (potential target) map was generated by the automated lineament detection output presenting the feature's orientation diversity and feature intersection on a density map (Figure 8). The circled areas clearly defined the increased features intersection density and features orientation diversity which is also the case in the findings reported by Holden et al. (2010). Further, the automatically produced structural complexity map highlights zones that were probably proximal to mineral deposits in the study area, especially the hydrothermal ones (Ekwok et al. 2020, Uwiduhaye et al. 2021). This can be proved by the presence of active gold mines and abandoned small-scale miners' pits in the study area (Figure 7). Potential targets were identified based on different geological structures trending in various directions. From the geophysical studies, the study area is divided into two geological units, the sedimentary and basement complex as reported by Kashabano et al. (2003). The basement complex is an area with favourable economic potential minerals like gold at Muhintiri and Shanta Gold Mine. These methods have resulted in the successful identification of geological structures that are viable for mineral exploration (Abdelrahman et al. 2023).
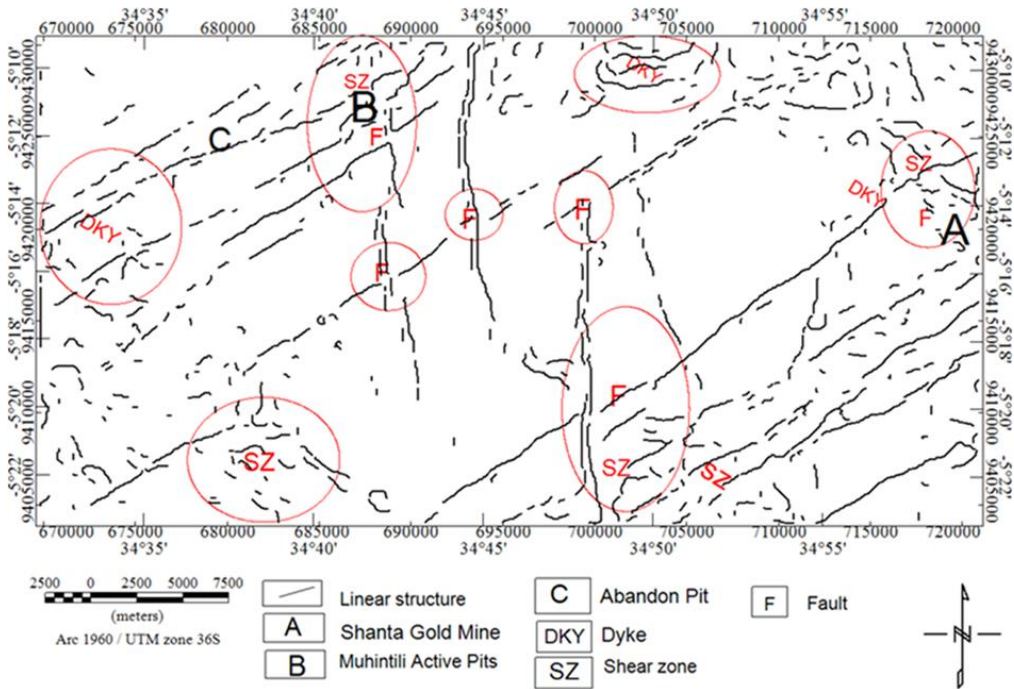
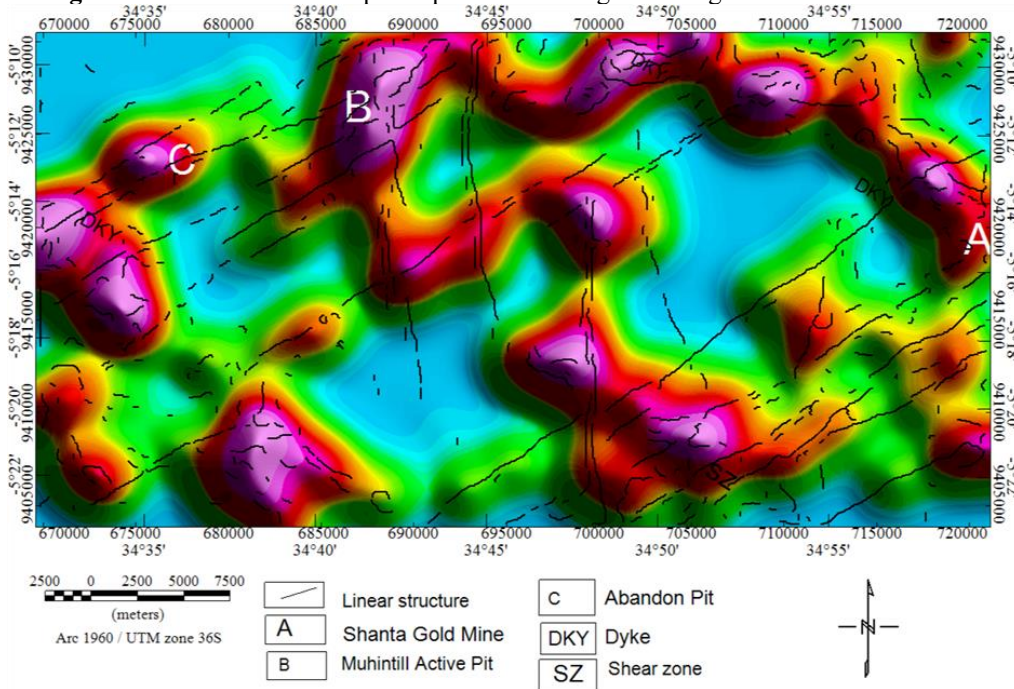**Figure 7**: Linear structure map interpreted from magnetic images.

Figure 8: Potential mineralized target with linear structures

Conclusions

The processed aeromagnetic data including the TMI, RTP, VD, and CET maps were used to infer the shallow and deep magnetized sources and associated structural elements. Several major faults, shear zones, and intrusive (dykes of different ages and extensions) were delineated. Three groups of

major linear structures such as shear zones, faults and fractures were identified as trending in NE-SW, N-S and NW-SE directions. Other faults/dykes, trending in the NE direction with a sense of lateral displacements resulting from shear zones were also mapped. Such structural elements probably act as favourable sites of mineral deposit potentials including gold. The CET technique identified mineralized zones, especially the structural intersections which form possible targets for mineral exploration. The integrating results of the present study with existing and ancient gold mines, and potential mineral occurrences (such as Shanta Gold Mine, abandoned pits, and the operating pits of small-scale miners in Muhintiri) correlated well with the detected structural complexities and faults intersections. Hence, this study recommends that areas which share similar characteristics with those that have demonstrated well correlation with gold occurrences/deposits should be prioritized for ground follow-up.

Acknowledgements

References

Abdelrahman K, El-Qassas RAY, Fnais MS *et al.* 2023 Geological structures controlling Au/Ba mineralization from aeromagnetic data: Harrat ad Danun Area, Saudi Arabia. *Minerals.* 13:866.

Alarifi SS, Kellogg JN and Ibrahim E 2019 Gravity, aeromagnetic and electromagnetic study of the gold and pyrite mineralized zones in the Haile Mine area, Kershaw, South Carolina. *J. Appl. Geophys.* 164: 117–129.

Ansari A and Alamdar K 2009 Reduction to the pole of magnetic anomalies using analytic signal. *World Appl. Sci. J.* 7(4):405-409.

Anudu GK, Stephenson RA and Macdonald DIM 2014 Using high-resolution aeromagnetic data to recognise and map intra-sedimentary volcanic rocks and geological structures across the Cretaceous middle Benue Trough, Nigeria. *J. Afr. Earth Sci,* 99:625-636.

Austin JR and Blenkinsop TG 2009 Local to regional scale structural controls on mineralisation and the importance of a major lineament in the eastern Mount Isa Inlier, Australia: Review and analysis with autocorrelation and weights of evidence. *Ore Geol. Rev.* 35(3-4):298-316.

Baranov V 1957 A new method for interpretation of aeromagnetic maps: 631 pseudo-gravimetric anomalies. *Geophysics* 22:359-382.

Barth H, Massola S and Weiser T 1996 Gold in the Dodoman basement of Tanzania. *Geol. Jahrb. B* 92, 53.

Bierlein FP, Murphy FC, Weinberg RF and Lees T 2006 Distribution of orogenic gold deposits in relation to fault zones and gravity gradients: targeting tools applied to the Eastern Goldfields, Yilgarn Craton, Western Australia. *Miner. Deposita* 41:107–126.

Blakely RJ 1995 *Potential Theory in Gravity and Magnetic Applications*, 649 Stanford-Cambridge Program. Cambridge University Press. 464pp.

Briggs IC 1974 Machine contouring using minimum curvature. *Geophysics,* 39:39-48.

Chernicoff CJ, Richards JP and Zappettini EO 2002 Crustal lineament control on magmatism and mineralisation in northwestern Argentina: geological, geophysical, and remote sensing evidence. *Ore Geol. Rev.* 21:127–155.

Cooper GRJ and Cowan DR 2004 Filtering using variable order vertical derivatives. *Comput. Geosci.* 30:455–459.

Cox SF, Knackstedt MA and Braun J 2001 Principles of structural control on permeability and fluid flow in hydrothermal systems. *Rev. Econ. Geol.* 14:1–24.

Cutten H, Johnson SP and Waele BD 2006 Protolith ages and timing of metasomatism related to the formation of Whiteschists at Mautia Hill, Tanzania: implications for the assembly of Gondwana. *J. Geol.* 114:683–

698.

Dentith M 2011 Magnetic methods, Airborne. In: Gupta, H.S. (Ed.), *Encyclopedia of solid earth geophysics,* vol. 1. Springer, Dordrecht, 761–766 pp.

Dentith M and Mudge ST 2014 *Geophysics for the Mineral Exploration Geoscientist*. Cambridge: Cambridge University Press.

Dobrin MB and Savit CH 1988 *Introduction to Geophysical Prospecting*, 4th edition, McGraw-Hill, New York. 867pp.

Ejepu J, Ako T and Abdullahi S 2018 Integrated geosciences prospecting for gold mineralization in Kwakuti, North-Central Nigeria. *J. Geol. Mining Res.* 10(7):81-94.

Ekwok SE, Akpan AE and Kudamnya EA 2020 Exploratory mapping of structures controlling mineralization in Southeast Nigeria using high resolution airborne magnetic data. *J. Afr. Earth Sci.* 162:103700.

Eldosouky AM, Elkhateeb SO, Ali A and Kharbish S 2020 Enhancing linear features in aeromagnetic data using directional horizontal gradient at Wadi Haimur area, South Eastern Desert, Egypt. *Carpathian J. Earth and Environ. Sci.* 15(2):323-326.

El-Qassas RA, Ahmed SB, Abd-ElSalam HF and Abu-Donia AM 2021 Integrating of remote sensing and airborne magnetic data to outline the geologic structural lineaments that controlled mineralization deposits for the area around Gabal El-Niteishat, central eastern desert, Egypt. *Geomaterials* 11(1):1-21.

Fossen H and Cavalcante GCG 2017 Shear zones–A review. *Earth-Sci. Rev.* 171:434-455.

Goldfarb RJ, Groves DI and Gardoll S 2001 Orogenic gold and geologic time: a global synthesis. *Ore Geol. Rev.* 18:1–75.

Groves DI, Goldfarb RJ, Gebre-Mariam M, Hagemann SG and Robert F 1998 Orogenic gold deposits: a proposed classification in the context of their crustal distribution and relationship to other gold deposit types. *Ore Geol. Rev.* 13:7–27.

Groves DI, Goldfarb RJ, Robert F and Hart CJR 2003 Gold deposits in metamorphic belts: overview of current understanding, outstanding problems, future research, and exploration significance. *Econ. Geol.* 98:1-29.

Heal P, McCuaig TC and Harris LB 2014 The Centre for Exploration Targeting: creating new paradigms for exploration targeting. *Aust. J. Earth Sci.* 61:635–40.

Holden EJ, Wong JC, Kovesi P, Wedge D, Dentith M and Bagas L 2012 Identifying structural complexity in aeromagnetic data: An image analysis approach to green fields gold exploration. *Ore Geol. Rev.* 46:47-59.

Holden EJ, Dentith M and Kovesi P 2010 CET Grid Analysis Extension.Available from Geosoft http://www.geosoft.com/about-geosoft/partners/geosoft-partner-network/cet.

Hronsky JMA and Groves DI 2008 The science of targeting: definition, strategies, targeting and performance measurement. *Aus. J. Earth Sci.* 55:2-12.

Jeffrey P, Hansen RO and Blakely RJ 2007 The use of curvature in potential-field interpretation. *Expl. Geophys. 38*(2):111-119.

Kabete J 2008 *A new terrane-based tectonic subdivision of the Archaean Craton and selected belts of Tanzania and its significance to gold metallogeny*. Unpublished PhD thesis. University of Dar es Salaam, 353pp.

Kabete JM, Gorves DI, McNaughton NJ and Mruma AH 2012b A new tectonic and temporal framework for the Tanzanian Shield: implications for gold metallogeny and undiscovered endowment. *Ore Geol. Rev.* 48: 88–124.

Kabete JM, McNaughton NJ, Groves DI and Mruma AH 2012a Reconnaissance SHRIMP U–Pb zircon geochronology of the Tanzania Craton: evidence for Neoarchean granitoid–greenstone belts in the Central Tanzania Region and the Southern East African Orogen. *Precambr. Res.* 216:232–266.

Kashabano JB, Semkiwa PM and Mbawal FLK 2003 *Brief explanation notes of QDS 122*. Dodoma: Geological Survey of Tanzania.

Kisters AFM, Kolb J, Meyer FM 1998 Gold

mineralization in high-grade metamorphic shear zones of the Renco mine, Southern Zimbabwe. *Econ. Geol*. 93:598-601.

Konadu AB, Dadzie I and Takyi-Kyeremeh K 2018 Integrating gravity and magnetic field data to delineate structurally controlled gold mineralization in the Sefwi Belt of Ghana. *J. Geophys. and Eng.* 15(4):1197-1203.

Kumwenda J and Lackie M 2019 Geophysical interpretation of the geology of the Stanthorpe region using aeromagnetic, gravity and radiometric data. *Explor. Geophys.* 50(6): 653–666.

Lam L, Lee SW and Suen CY 1992 Thinning methodologies - a comprehensive survey, *IEEE Trans. Pattern Anal. Mach. Intell.* 14 (9):869-885.

Luyendyk APJ 1997 Processing of Airborne Magnetic Data. AGSO, *J. Aust. Geol. Geophys*. 17:31-38.

Milligan PR and Gunn PJ 1997 Enhancement and Presentation of Airborne Geophysical Data. *J. Aust. Geol.& Geophys.* 17:63-75.

Msechu MHM 2019 *Briefly Explanatory notes of Geology of QDS 122.* Dodoma: Geological Survey of Tanzania.

Reynolds JM 2011 *An Introduction to Applied and Environmental Geophysics*. Second Ed., Wiley-Blackwell, West Sussex. 696pp.

Semkiwa P and Myumbilwa Y 2013 Geology and Geochemistry of the Area Around Sambaru, Londoni and Msangachuki Gold Prospect. *Tanz. J. Earth Sci.* 2:3-13.

Sibson RH, Robert F and Poulsen KH 1988 High-angle reverse faults, fluid pressure cycling and mesothermal gold quartz deposits. *Geol.* 16:551–555.

Sillitoe RH 2000 Gold-rich porphyry deposits: descriptive and genetic models and their role in exploration and discovery. *Rev. Econom. Geol.* 13:315–345.

Smith J, Brown C, Blackwell M *et al.* 2019 Application of CET tools to mapping geological structures in challenging terrain. *J. Appl. Geophys.* 161:132–44.

Swain CJ 1976 A Fortran IV program for interpolating irregularly spaced data using the difference equations for minimum curvature. *Comput. Geosci.* 1:231-240.

Tawey MD, Udensi EE, Adetona AA and Alhassan UD 2019 Delineation of Mineralization Zones in Part of Central Nigeria Using Analytic Signal, Second Vertical Derivative, and Centre for Exploration Targeting Plug-IN (CET). *Int. J. Sci. Global Sustain*. 5(1):10-10.

Telford WM, Geldart LP and Sheriff RE 1998 *Applied Geophysics*, Second Ed. Springer, 770pp.

Thomas RJ, Bushi AM, Roberts NMW and Jacobs J 2014 Geochronology of granitic rocks from the Ruangwa region, southern Tanzania – links with NE Mozambique and beyond. *J. Afr. Earth Sci.* 100:70–80.

Thomas RJ, Roberts NMW, Jacobs J, Bushi AM, Horstwood MSA and Mruma A 2013 Structural and geochronological constraints on the evolution of the eastern margin of the Tanzania Craton in the Mpwapwa area, central Tanzania. *Precambr. Res.* 224:671–689.

Tounkara F, Chen J and Keita S 2017 Integrated Interpretation of Geophysical and Soil Geochemical Anomalies in Gold Exploration: Case of Kouremale, Southern Mali-West Africa. *Inter. J. Geosci.* 8(9):1133–1145.

Uwiduhaye JD, Ngaruye JC and Saibi H 2021 Defining potential mineral exploration from the interpretation of aeromagnetic data in Western Rwanda. *Ore Geol. Rev.* **128**:103927.

Verduzco B, Fairhead JD, Green CM and MacKenzie C 2004 New insights into magnetic derivatives for structural mapping. *The Leading Edge* 23(2):116-119.